ARMY RESEARCH LABORATORY

An Elementary Electron Model for Electron-Electron Scattering Based On Static Magnetic Field Energy

Harry J. Auvermann

ARL-TR-2332

February 2001

The findings in this report are not to be construed as an official Department of the Army position unless so designated by other authorized documents.

Citation of manufacturer's or trade names does not constitute an official endorsement or approval of the use thereof.

Destroy this report when it is no longer needed. Do not return it to the originator.

Army Research Laboratory

Adelphi, MD 20783-1197

ARL-TR-2332 February 2001

An Elementary Electron Model for Electron-Electron Scattering Based On Static Magnetic Field Energy

Harry J. Auvermann

Computational and Information Sciences Directorate

Abstract

Electron motion paths that exhibit zero radiation in a Maxwells equation solution have been reported. Such paths, require a radiationless model of the electron itself, such as the charged hollow sphere. When the electric-field energy of this model is set equal to the rest mass energy of the electron, the radius of the resulting sphere is called the "classical electron radius." Analysis reveals that the static magnetic-field energy of the classical model is many times the electron rest mass energy when the sphere is given an angular velocity large enough to exhibit the electron magnetic moment. The necessary angular velocity produces a peripheral velocity many times the speed of light. A classical model with a peripheral velocity near the speed of light is a loop whose radius is the Compton wavelength divided by 2π; such a loop has a very small dimension perpendicular to the loop plane. Experiments reveal point-like electron scattering properties down to at least 1/100 of the classical radius. The small transverse dimensions of the loop model indicate similar scattering results. Recently, a proposal was submitted to investigate the scattering properties of interacting loops. Because of limited proposal length, derivation of loop model equations could not be included. This report contains the details of the analysis.

Contents

Figures

1. Introduction

When the Bohr atom is introduced in a physics curriculum, the derivation of the constants of motion for the electron proceeds by assuming this moving charge does not radiate as it traverses the circular or elliptical orbit, even though an accelerating charge is known to radiate energy according to Maxwell's equations. I have always been intrigued by the problem of finding radiationless charge-current distributions but did no serious investigation until I discovered an article published in 1964 [1]. The following quote is a transcription of the first two paragraphs of the introduction from this article:*

"It still seems a fairly common belief that there exist no nontrivial charge-current distributions which do not radiate, according to classical electromagnetic theory retarded potential solutions. However, early in this century Sommerfeld,[1] Herglotz,[2] and Hertz[3] considered extended electron models, and established the existence of radiationless self-oscillations. In 1933, Schott[4] showed that a uniformly charged spherical shell will not radiate while in orbital motion with period T, provided the shell radius is an integral multiple of $cT/2$; the orbit need not be circular nor even planar. In 1948, Bohm and Weinstein[5] found several other rigid spherically symmetric distributions that can oscillate linearly without radiating.

In this paper we derive a simple exact criterion for absence of radiation, and apply it to moving rigid extended charge distributions.[6] We find that there are many such distributions, some of which may "spin," and others which need not be spherically symmetric. The allowed types of such distributions are severely restricted by the condition of no radiation; further, it must be true that the finite radius of a rigid volume distribution be an integer multiple of cT, where T is the period of orbital motion. This last restriction implies that the perimeter of the orbit is less than the extent of the distribution.[4]"

Encouraged by these published results, I began an effort to find a radiationless alternative to the "Solar System-like" orbits of the Bohr atom during the year (1968–1969) that I held a temporary appointment in the Physics

*The following are the references cited in Goedecke's article.

[1] A. Sommerfeld, Nachr. Akad. Wiss. Goettingen, Math.-Physik, Kl. IIa Math.-Physik. Chem. Abt. 1904, 99 and 363; 1905, 201.

[2] G. Herglotz, Nachr. Akad. Wiss. Goettingen, Math.-Physik, Kl. IIa Math.-Physik. Chem. Abt. 1903, 357; *Math. Ann.* **65**, 87 (1908).

[3] P. Hertz, *Math. Ann.* **65**, 1 (1908).

[4] G. A. Schott, *Phil. Mag. Suppl.* 7 **15**, 752 (1933).

[5] D. Bohm and M. Weinstein, *Phys. Rev.* **74**, 1789 (1948).

[6] In *Bull. Am. Phys. Soc.* **9**, 148 (1964), "which I [Goedecke] received while writing this paper, there appears an abstract by S. M. Prastein and T. Erber which implies that some of the content of this paper has been worked out independently by these authors."

Department of The University of Texas at Arlington. One can quickly conclude that a necessary part of producing a radiationless model of the hydrogen atom is a radiationless model of the electron. I therefore began a study of the properties of the electron with the simple derivation of the classical radius. The semiclassical derivation for this quantity equates the static electric-field energy of a hollow sphere, bearing the electron charge to the rest mass energy. As a part of my education, I examined the static magnetic-field energy of a spinning sphere whose radius is the classical radius, expecting that the magnetic-field energy would be much less than the classical electric-field energy. Using my own approximation for the magnetic-field energy, I was quite surprised to find that the magnetic-field energy was some 900 times the electric-field energy. Additionally, the peripheral velocity of the sphere had to be many times the speed of light to achieve the required magnetic moment. Backing off from the classical radius requirement, I sought the radius of a charged loop whose peripheral velocity was the speed of light but still had the correct magnetic moment and field energy. My calculation, although approximate, resulted in the model loop radius being what I call the "Compton radius," the latter being the radius of a circle whose circumference is the Compton wavelength.

At this juncture, I made one further calculation. I determined approximately that the required "charged wire" radius to give an electric-field energy for a Compton radius-sized loop to be equal to the electron rest mass was a number so small that it defied imagination. Other pressures caused me to abandon the work on this project, but I have continued to think about it. One significant event in this connection occurred perhaps in the early 90s. This event was the report that a colliding beam experiment, I believe the European Organization for Nuclear Research (CERN), showed that the cross section for electron-electron scattering was spherical to at least a factor of 100 less than the classical size. I have not relocated the reference to this report to verify this result, but I have been assured by two colleagues that this result is currently universally accepted in the particle physics community. Because of my "charged wire" radius calculation, I wondered when the experiment report came out if this might somehow indicate that I was on the right track with my Compton radius loop model.

I have described the events up to when the notice of the current director's research initiative (DRI) was circulated. Since I have been intrigued by this problem of finding radiationless charge-current distributions, I derived anew my previous results before submitting my proposal on 14 July 2000 to investigate the scattering properties of interacting current loops. A copy of the proposal has been included as appendix A. This report contains the derivation including an improved magnetic-field energy expression. Also included in this report, but not in the proposal, is a classical calculation of the potential energy necessary to bring two Compton radius loops to a separation distance equal to a small fraction of the classical radius.

2. Equations for Physical Constants

A recent article [2] presents the latest information on the fundamental constants. Equations for physical constants in terms of fundamental constants are presented here. The fine structure constant [2, p 448] is

$$\alpha = \left(\frac{\mu_0 c^2}{4\pi}\right)\left(\frac{(2\pi)e^2}{hc}\right) = \left(\frac{(2\pi)e^2}{4\pi\varepsilon_0 hc}\right) , \tag{1}$$

where e is the electronic charge, h is Planck's constant, and c is the speed of light in vacuum. The Bohr radius [2, p 448] is given as

$$a_0 = \left(\frac{\mu_0 c^2}{4\pi}\right)^{-1}\left(\frac{h^2}{(2\pi)^2 m_e e^2}\right) , \tag{2}$$

where m_e is electron rest mass. The classical electron radius [2, p 449] is

$$r_0 = \left(\frac{\mu_0 c^2}{4\pi}\right)\left(\frac{e^2}{m_e c^2}\right) . \tag{3}$$

The Bohr magneton [2, p 448] is

$$\mu_B = \left(\frac{eh}{4\pi m_e}\right) . \tag{4}$$

The Compton wavelength of the electron [2, p 449] is

$$\lambda_C = \left(\frac{h}{m_e c}\right) . \tag{5}$$

For this derivation, a quantity that I call the "Compton radius" is defined as the radius of the circle whose circumference is the Compton wavelength,

$$r_C = \left(\frac{h}{2\pi m_e c}\right) . \tag{6}$$

Note that these three radii are related through the fine structure constant

$$\frac{r_C}{a_o} = \frac{r_0}{r_C} = \alpha . \tag{7}$$

The energy represented by the electron rest mass is

$$w_e = m_e c^2 . \tag{8}$$

From the electromagnetic wave equation, the magnetic constant μ_0 and electric constant ε_0 are related to c [2, p 448],

$$c^2 = \frac{1}{\mu_0 \varepsilon_0} . \tag{9}$$

The potential of a point of charge q at a distance r [3, p 312] is

$$\phi_s = \frac{q}{4\pi\varepsilon_0 r} \,. \tag{10}$$

By multiplying equation (10) by the charge and setting the left-hand side equal to the rest mass energy of the electron and then the charge on the right-hand side equal to the electronic charge, one can define the resulting radius to be the classical radius of the electron.

3. Magnetic-Field Energy of a Spherical Shell Electron Model

The next step is to spin the electron modeled as a charged shell and to determine the magnetic moment of this configuration. An approximation for the magnetic moment of a spinning charged sphere has been derived in appendix B in terms of an equivalent current loop. Equation (11) is an adaptation of equation (B-6) in the appendix, where the superscript s indicates that the variables are those of the sphere and v^s is the peripheral velocity of the sphere:

$$\mu^s = \frac{2r_e q^s v^s}{3} \,. \tag{11}$$

The free electron g-factor [2, p 449], or electron magnetic moment μ_e in Bohr magnetons, is

$$\frac{g_j}{2} = \frac{\mu_e}{\mu_B} \,. \tag{12}$$

Using this relation and setting the sphere magnetic moment equal to the electron magnetic moment allow the rotational velocity to be isolated as

$$v^s = \frac{3g_j\mu_B}{4r_e e} \,. \tag{13}$$

Substitution for the known quantities from section 2 produces the velocity in terms of fundamental constants as

$$v^s = \left(\frac{3}{4}\right)\left(\frac{g_j}{2}\right)\left(\frac{c}{\alpha}\right) \,. \tag{14}$$

It is instructive to estimate the multiplier of c, which here gives the peripheral velocity of this model. The fine structure constant in the denominator produces a factor of about 137 in the numerator, and the free electron g-factor is about 1. Thus, the peripheral velocity is upward of 100 times the speed of light, a truly astonishing result. The sense of this calculation is that a current loop with a radius equal to the classical electron radius must have a velocity inconsistent with relativity theory to exhibit the measured electron magnetic moment.

Another comparison may be made with this equivalent current loop model. This comparison calculates the magnetic-field energy of the equivalent current loop. The general expressions for the inductance of a loop [3, p 326] and for the energy stored in the inductance of a circuit [3, p 327] are

$$\begin{aligned} L_g &= b\left[\mu\left(\ln\left(\frac{8b}{a}\right) - 2\right) + \frac{\mu'}{4}\right] \;; \quad \text{Let } \mu' = \mu \\ L_g &= C_g(\rho_g)\mu b \;; \quad C_g(\rho_g) = \ln(d_g\rho_g) \\ &\qquad \rho_g = \frac{b}{a} \;; \quad d_g = 8\exp\left(-\frac{7}{4}\right) \geq 1.39 \\ w_{\text{circuit}} &= \frac{L_{\text{circuit}} I^2_{\text{circuit}}}{2} \,, \end{aligned} \tag{15}$$

where L_g is the inductance of a general loop, b is the radius of the loop, a is the radius of the wire, μ is the medium permeability, and μ' is the permeability of the wire. Also w_{circuit} is the circuit energy, L_{circuit} is the circuit inductance, and I_{circuit} is the circuit current. Assuming that the wire permeability is the same as that of the medium permits the simplification shown in the second line of equation (15). Replacing the general loop dimensions of equation (15) with the dimensions of the equivalent loop gives the inductance L_s^{eq} of the loop equivalent to the spinning sphere

$$L_s^{\text{eq}} = C_g(\rho_s)\mu_0 r_0 \; ; \qquad \rho_s = \frac{r_0}{r_t} \, . \tag{16}$$

The quantity $C_g(\rho_s)$ involves the natural logarithm of the ratio of the classical electron radius to the radius r_t, which is an unspecified radius of the torus tube containing the charge and corresponds to the wire radius a. This quantity is thus related to the assumed configuration of the loop and does not change with the loop radius if the configuration remains the same. The minimum value of the parameter ρ_s is one so that the minimum value of this factor is ln(1.39) = 0.329.

The field energy expression of equation (15) may now be used wherein the energy of the equivalent loop w_s^{eq} is substituted for w_{circuit}, the equivalent inductance from equation (16) is substituted for L_{circuit}, and the equivalent current I_s^{eq} is substituted for I_{circuit}. With all relevant quantities brought together, the magnetic energy of the spinning shell model of the electron will be

$$\begin{aligned} w_s^{\text{eq}} &= \frac{L_s^{\text{eq}}(I_s^{\text{eq}})^2}{2}; \quad L_s^{\text{eq}} = C_g(\rho_s)\mu_0 r_0; \quad I_s^{\text{eq}} = \left(\frac{e\nu^s}{2\pi r_0}\right) \\ &= \left(\frac{C_g(\rho_s)\mu_0 r_0}{2}\right)\left(\frac{3g_j ec}{8(2\pi)r_0\alpha}\right)^2; \quad \nu^s = \frac{3g_j c}{8\alpha} \\ &= \left(\frac{9C_g(\rho_s)\mu_0(g_j)^2 r_0}{128(2\pi)^2}\right)\left(\frac{ec}{\alpha r_0}\right)^2 . \end{aligned} \tag{17}$$

Rearranging and substituting give the result

$$\begin{aligned} w_s^{\text{eq}} &= \left(\frac{9C_g(\rho_s)(g_j)^2\mu_0 r_0}{128(2\pi)^2}\right)\left(\frac{ec}{\alpha r_0}\right)^2 = \Lambda(\rho_s)\left(\frac{\mu_0 r_0}{4(2\pi)^2}\right)\left(\frac{ec}{\alpha r_0}\right)^2 \\ &= \Lambda(\rho_s)\left(\frac{\mu_0 e^2 c^2}{(4\pi)^2\alpha^2 r_0}\right) = \Lambda(\rho_s)\left(\frac{e^2}{(4\pi)^2\varepsilon_0\alpha^2 r_0}\right) \\ &= \Lambda(\rho_s)\left(\frac{w_e}{4\pi\alpha^2}\right); \quad \Lambda(\rho_s) = \left(\frac{9C_s^L(\rho_s)}{8}\right)\left(\frac{g_j}{2}\right)^2 . \end{aligned} \tag{18}$$

Here, the magnetic field energy with the use of the spherical model (estimated in eq (18)) is very much more than the experimentally determined rest mass energy of the electron. Aside from the dimensionless quantity $\Lambda(\rho_s)$, which is about 3/8 as a minimum, the numerical factor $(4\pi\alpha^2)^{-1}$ is about 1494.

4. Properties and Configuration of Loop Electron Model

In this section, the formalism presented in section 3 is used to determine the radius of a current ring whose energy is equal to the rest mass energy of the electron under the condition that the magnetic moment of the ring is equal to the magnetic moment of the electron. The radius of the ring as determined will be identified with the symbol $r_m^{\rm cl}$ with the other variables used in the derivation identified with a similar subscript-superscript pair. The eventual equation to be solved is

$$\begin{aligned} L_m^{\rm cl} &= C_m^{\rm cl}(\rho_m)\mu_0 r_m^{\rm cl}\ ;\ \rho_m = \frac{r_m^{\rm cl}}{r_m} \\ w_m^{\rm cl} &= \frac{L_m^{\rm cl}(I_m^{\rm cl})^2}{2}\ ; \qquad w_m^{\rm cl} = m_e c^2 \end{aligned} \tag{19}$$

where r_m is the torus tube radius for the magnetic loop.

The magnetic moment equation is

$$\begin{aligned} \mu_m^{\rm cl} &= \mu_e = \frac{g_j \mu_B}{2} \\ \mu_m^{\rm cl} &= A_m^{\rm cl} I_m^{\rm cl}\ ;\quad A_m^{\rm cl} = \pi (r_m^{\rm cl})^2\ ;\quad I_m^{\rm cl} = \left(\frac{e v_m^{\rm cl}}{2\pi r_m^{\rm cl}}\right)\ . \end{aligned} \tag{20}$$

From equations (19) and (20), the current is eliminated as in

$$m_e c^2 = \frac{C_g(\rho_m)\mu_0 r_m^{\rm cl}(I_m^{\rm cl})^2}{2} = \left(\frac{C_g(\rho_m)\mu_0 r_m^{\rm cl}}{2}\right)\left(\frac{g_j \mu_B}{2\pi (r_m^{\rm cl})^2}\right)^2\ . \tag{21}$$

The solution for the radius is obtained by rearranging equation (21) as

$$r_m^{\rm cl} = \left(\frac{C_g(\rho_m)\mu_0 (g_j \mu_B)^2}{2(2\pi)^2 m_e c^2}\right)^{1/3} = \left(\frac{C_g(\rho_m)\mu_0 (g_j)^2 (eh)^2}{2(2\pi)^2 m_e c^2 (4\pi m_e)^2}\right)^{1/3}\ . \tag{22}$$

One way to analyze the expression on the right in equation (22) is to extract a factor equivalent to the Compton radius as

$$r_m^{\rm cl} = \left(\frac{C_g(\rho_m)\mu_0 (g_j)^2 (eh)^2}{2(2\pi)^2 m_e c^2 (4\pi m_e)^2}\right)^{1/3} = \left(\frac{h}{2\pi m_e c}\right)\left(\frac{C_g(\rho_m)(g_j/2)^2 \alpha}{2\pi}\right)^{1/3}\ . \tag{23}$$

The magnetic radius is thus seen to be the Compton radius times a factor that is not a function of the loop radius but rather is a function of the quantity ρ_m, which is the ratio of the loop radius to the torus radius. The latter is an indicator of the extent of the loop dimension parallel to the loop axis. To

gain insight to the magnitude of this torus radius, determine the velocity of the loop charge for the case of $r_m^{\rm cl} = r_C$. This is obtained from the relation

$$\begin{aligned} \mu_e &= \frac{r_m^{\rm cl} e v_m^{\rm cl}}{2} \; ; \quad v_m^{\rm cl} = \frac{2\mu_e}{r_m^{\rm cl} e} \\ v_m^{\rm cl} &= \frac{g_j \mu_B}{r_m^{\rm cl} e} = \left(\frac{g_j}{r_m^{\rm cl} e}\right)\left(\frac{eh}{4\pi m_e}\right) . \end{aligned} \tag{24}$$

With the substitution for the Compton radius, the result is

$$v_m^{\rm cl} = \left(\frac{h g_j}{4\pi m_e}\right)\left(\frac{1}{r_C}\right) = \left(\frac{h g_j}{4\pi m_e}\right)\left(\frac{2\pi m_e c}{h}\right) = (g_j/2)c \, . \tag{25}$$

This shows that the resulting velocity of the loop charge is near the velocity of light if the loop radius is the Compton radius. Assuming this calculation is accurate enough, one may determine the loop configuration parameter ρ_m from

$$\begin{aligned} \left(\frac{C_g(\rho_m)\alpha}{2\pi}\right)^{1/3} &= 1 \\ C_m^{\rm cl}(\rho_m) &= \frac{2\pi}{\alpha} = \ln(d_g \rho_m) \\ \rho_m &= \exp\left(\frac{2\pi}{\alpha} + \frac{7}{4} - \ln(8)\right) \cong \exp(2\pi 137) \cong e^{861} \, . \end{aligned} \tag{26}$$

What is astonishing about this estimate is that the indicated torus tube radius is so incredibly minute.

5. Loop Electron Model Related to Experimental Findings

In section 4, I have shown that a current loop structure whose radius is the Compton radius satisfies the magnetic moment and the rest mass energy requirements necessary to model an electron. Furthermore, such a structure has the potential to reproduce the electron-electron scattering cross-section results reported in the literature. I make this statement because the indicated dimension of the current loop model in the direction perpendicular to the loop plane is quite small. The scattering geometry for two colliding loops is so complex that just what happens as they approach each other is not readily apparent for the general case with arbitrary orientation of the two magnetic moments and arbitrary displacement of the loop center paths. However, for coaxial center paths with orientation such that the paths are perpendicular to the planes of the two loops and for only classical electric-field interaction, a distance of closest approach equal to that reported in the experiment can be achieved for the two loops. Thus, in the backscatter direction, the scattering is appropriate within the framework imposed by the provisos in the previous sentence.

From my previous approximate calculation of the "charged wire" radius alluded to in the introduction of section 1, the torus radius is so small that the electric-field energy necessary to compress the charge into a torus of this size may rival the computed magnetic energy. This then indicates that the distribution of the electron rest mass energy between the electric and magnetic fields may be useful in suggesting further modifications of the configuration of a classical model of the electron. Accounting for relativistic effects more completely will be necessary in further modifications of the loop model also. It may be necessary to introduce periodic motions of the loop to realize the radiationless restriction. One possible motion is the rotation of the loop about an axis inclined with respect to the magnetic moment. Additionally, accounting for the spin angular momentum may require further modifications.

These thoughts are presented to emphasize that a current loop model of the electron is just that, a model. Elaborations are expected to be necessary. In this same spirit, it is not prudent to attempt these elaborations before the more elementary configurations are investigated as to their scattering properties. Thus, the objective of the DRI proposal was to investigate the scattering properties of progressively more complex models in the geometry of the recorded experiment. The a priori expectation is that some of the general features of the experimental findings will be present with the use of the simplest model. On the other hand, a full relativistic treatment, including both electric and magnetic interactions, may be needed. As far as what is known at present, no exposition of the theory for loop-loop scattering exists.

6. Potential Energy Results for Two Interacting Charged Loops

This section compares the potential energy of the current loop electron model in the interaction geometry described in appendix C with the potential energy of the spherical shell electron model. The potential energy of the spherical shell model $W^e_{AB}(p)$ is given as

$$W^e_{AB}(p) = -\int_{\infty}^{p} dr \left(\frac{q_a^2}{4\pi\varepsilon_0 r^2}\right) = \left(\frac{q_a^2}{4\pi\varepsilon_0 p}\right) . \tag{27}$$

In the equation, the radius of the shell r_s is not specified. If $r_s < p < r_0$, which is the condition imposed upon the shell model by the experimental results, the field energy must be larger than the measured rest mass energy of the electron. With this in mind, one can base the comparison upon the shell model energy for a separation of the Bohr radius r_B given by [2]

$$r_B = \left(\frac{4\pi\varepsilon_0 h^2}{(2\pi)^2 m_e q_a^2}\right); \quad \alpha = \left(\frac{(2\pi)q_a^2}{4\pi\varepsilon_0 hc}\right) . \tag{28}$$

Also shown in equation (28) is the expression for the fine structure constant α [2]. The constants used in this derivation are shown in relation to the Bohr radius as

$$\begin{aligned} \text{Compton radius} &= r_C = r_m^{\text{cl}} = a = \alpha r_B \\ \text{Classical radius} &= r_0 = \alpha^2 r_B \\ \text{Nearest approach distance} &= p_n = \alpha^3 r_B \\ \text{Nearest approach parameter} &= q_n = \alpha^2/2 . \end{aligned} \tag{29}$$

The reference energy W_R is defined in equation (30) by the insertion of equation (28) into equation (27):

$$W_R = m_e \left(\frac{(2\pi)q_a^2}{4\pi\varepsilon_0 h}\right)^2 = m_e c^2 \alpha^2 . \tag{30}$$

In equation (31), both equation (C-13) from appendix C for the interaction potential energy for the loop model $W^m_{AB}(p)$ and equation (27) are rewritten in terms of equation (30):

$$\begin{aligned} W^m_{AB}(p) &= \left(\frac{2k^{1/2} q_a^2 K(k)}{(2\pi)4\pi\varepsilon_0 a}\right) = W_R \left(\frac{2k^{1/2} K(k)}{(2\pi)\alpha}\right) \\ W^e_{AB}(p) &= \int_{\infty}^{p} dr \left(\frac{q_a^2}{4\pi\varepsilon_0 r^2}\right) = W_R \left(\frac{p}{r_B}\right)^{-1} . \end{aligned} \tag{31}$$

I have defined several symbols in equation (32) to simplify notation for presentation of the data:

$$\begin{aligned}\Xi^m(\bar{p}) &= \frac{W^m_{AB}(p)}{W_R} = \left(\frac{2\kappa(\bar{p})^{1/2}K(\kappa(\bar{p}))}{(2\pi)\alpha}\right); \quad \kappa(\bar{p}) = \left(\frac{1}{1+(2\alpha)^{-2}\bar{p}^2}\right) \\ \Xi^e(\bar{p}) &= \frac{W^e_{AB}(p)}{W_R} = \bar{p}^{-1}; \quad \bar{p} = \left(\frac{p}{r_B}\right). \end{aligned} \tag{32}$$

One more step is taken to place the data in a proper perspective, such as

$$\begin{aligned}\overline{W}^m(\xi) &= \Xi^m(\bar{p}) = \left(\frac{2\bar{\kappa}^{1/2}K(\bar{\kappa})}{(2\pi)\alpha}\right); \quad \bar{\kappa} = \left(\frac{1}{1+(2\alpha)^{-2}\xi^{-2\log(\alpha)}}\right) \\ \overline{W}^e(\xi) &= \Xi^e(\bar{p}) = \xi^{-\log(\alpha)}; \quad \xi = \bar{p}^{-1/\log(\alpha)}; \quad \alpha = 10^{\log(\alpha)}. \end{aligned} \tag{33}$$

A new variable ξ is introduced that represents the distance of nearest approach. This variable is designed to emphasize the sweep of the distances being considered. With this choice of the abscissa variable, the relation between the two relative energy functions at the separation points of $p = r_B, r_C, r_0, p_n$ occurs at the variable values of $\xi = 1, 10^{-1}, 10^{-2}, 10^{-3}$, respectively. Results calculated from the expressions in equation (33) are shown in figure 1. The essence of these results is displayed on the left side of the figure that corresponds to a minimum separation of p_n from equation (29). The graph shows that the energy required to bring the spherical model electron to this distance of nearest separation is some 4 orders of magnitude greater than that required to bring the loop model of the electron to the same distance of nearest separation. It is instructive to record some of the absolute numbers associated with the interaction under investigation. The fundamental constants [2] are

$$\begin{aligned}\alpha &= 0.00729735 = \text{fine structure constant} \\ m_e &= 9.10939 \times 10^{-31}\,\text{kg} = \text{electron rest mass} \\ c &= 299792458\ \text{m/s}^{-1} = \text{speed of light} \\ e &= 1.60218 \times 10^{-19}\,\text{C} = \text{electronic charge} \\ r_B &= 5.29177 \times 10^{-11}\,\text{m} = \text{Bohr radius}. \end{aligned} \tag{34}$$

The value of the electronic charge is only needed to convert from Joules to electron volts. Derived quantities and the calculated relative potential energies are

$$\begin{aligned} p_n &= \alpha^3 r_B = 2.056350 \times 10^{-17}\,\text{m} \\ W_R &= m_e c^2 \alpha^2 = 4.3597 \times 10^{-18}\,\text{J} = 27.2114\ \text{electron volt} \\ \overline{W}^e(r_B) &= 1.00; \qquad \overline{W}^e(p_n) = 2.573380 \times 10^6 \\ \overline{W}^m(r_B) &= 9.999468 \times 10^{-1}; \qquad \overline{W}^m(p_n) = 5.199462 \times 10^2. \end{aligned} \tag{35}$$

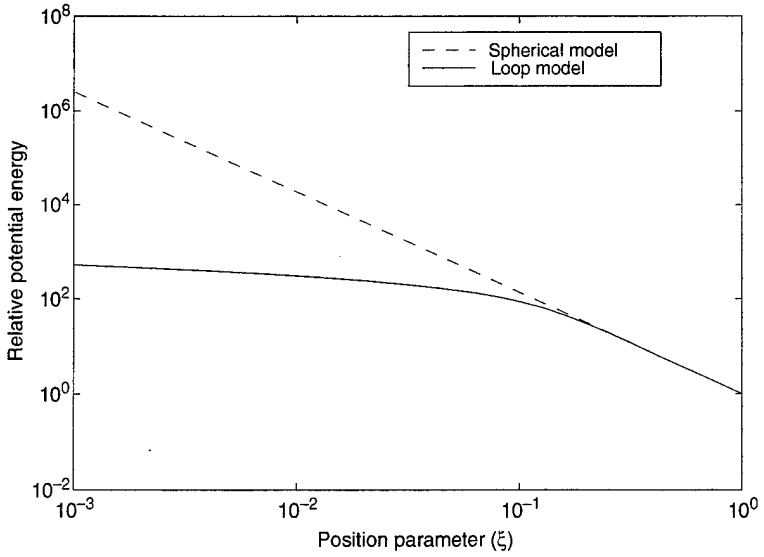

Figure 1. Relative interaction potential energy for two electron models.

Absolute potential energies are

$$\begin{aligned} W^{e}_{AB}(r_B) &= 4.3597 \times 10^{-18}\,\mathrm{J} = 27.2114 \text{ electron volt} \\ W^{m}_{AB}(r_B) &= 4.3594 \times 10^{-18}\,\mathrm{J} = 27.2100 \text{ electron volt} \\ W^{e}_{AB}(p_n) &= 1.1219 \times 10^{-11}\,\mathrm{J} = 70.0253 \times 10^{6} \text{ electron volt} \\ W^{m}_{AB}(p_n) &= 2.2668 \times 10^{-15}\,\mathrm{J} = 1.4148 \times 10^{4} \text{ electron volt}\,. \end{aligned} \tag{36}$$

Of particular interest in the results shown in equation (36) is the order of magnitude of the energy that must be supplied to bring two electrons to within the separation distance of a fraction of the classical radius of $r_0 = 2.8179 \times 10^{-15}$ according to the two models. Whereas, the spherical model indicates 70,000,000 electron volts, the loop model shows some 14,000 electron volts.

7. Summary and Discussion of Results

The classical physics calculations of this report started with the spherical shell model of the electron for which the classical radius is calculated by equating the electric-field energy to the measured electron rest mass energy. Assuming this sphere was spinning fast enough to generate a magnetic moment equal to its measured value, I showed that the peripheral velocity required would be many times the speed of light. Furthermore, I also showed that the magnetic-field energy of such a magnetic moment would be some 1000 times the rest mass energy. The quantity then sought was the radius of some object (probably a loop) whose peripheral velocity was near the speed of light (equal to it in the derivation) and, at the same time, giving the correct magnetic moment and the correct magnetic-field energy. The resulting object was a torus whose radius was proportional to the Compton wavelength divided by 2π—the latter quantity is being referred to as the magnetic radius r_m^{cl}. The proportionality factor was the cube root of the natural logarithm of the torus radius divided by the toroidal tube radius r_m. Selecting a value for this proportionality factor implied a rudimentary structure. If the value selected is unity, then the tube radius is uncommonly small. If, on the other hand, a value is selected less than unity, while the tube radius is increased, the loop radius is decreased from the magnetic radius, which in turn requires a peripheral velocity greater than the speed of light. I calculated further results using the proportionality factor of unity.

At this point, I include modern experimental results in the calculations. It is widely understood that high-energy electron-electron scattering experiments show that the scattering pattern is that of a point like entity down to several orders of magnitude less than the classical radius. Since the indicated tube radius r_m is so small, the speculation arises as to the scattering pattern of such a loop. The first step in such an investigation was performed in this report. The potential interaction energy was calculated under the assumption of only electric-field forces. The arrangement of the coaxial interacting loops was that their planes were parallel and that the direction of approach was perpendicular to these planes. Calculations showed that the potential energy of the spherical model was about 4 orders of magnitude greater than that of the loop model at the nearest approach distance chosen. Thus, to the limited extent suggested by the primitive interaction scenario used in this report, the loop model results are in accordance with the experimental results.

While no definitive theory has yet been applied to calculate interaction parameters for alternate (and more realistic) scenarios, one can reach certain conclusions by starting from the nature of the force fields involved. Some of these conclusions concerning alternate scenarios pertinent to further work follow:

- Scenario 1: Loops approach in planes perpendicular to approach line (electric and magnetic forces). Magnetic forces will have dramatic influences, especially since the interaction force is attractive if the magnetic moments are in the same direction. The relation between electric and magnetic forces as a function of separation is the priority calculation needed because the results will show if magnetic forces must be used in the following scenarios. An aspect of this relation was indicated by an approximate calculation done some time ago. This calculation was used to judge the radius of a charged torus tube necessary for the electric-field energy to be the rest mass energy. The rough results showed this radius to be very small also. An improved calculation of this effect has been included in appendix D, where it is indeed shown that the electric-field energy of a hollow torus is the electron rest mass energy. This information could not be used in this report because an appropriate partition of the energy between the electric and magnetic fields has not been determined.

- Scenario 2: Loops approach "edge one" (electric field). The nearest approach distance will be nearly twice the loop radius. Since the interaction force is higher for the nearest arc segments of the loops than it is for the farther separated arc segments, the scenario is unstable because of the torque involved. Any alignment error will tend to increase the error until the loops are parallel. This unstable approach alignment will have a very low probability and therefore contribute little to an averaged scattering cross section.

- Scenario 3: Loop centers on approach line—planes are not perpendular to approach line (electric forces). Here also torque will be exerted on each loop by the field of the other because of the different distances between loop segments. The torque will tend to rotate the loops into parallel plane alignment at the point of nearest approach after which the torque will reverse the rotation. There is a dynamic effect here, since the torque depends upon the relative orientation angle, which is the angle being changed by the integral of the torque times the moment of inertia.

- Scenario 4: Loop center not on same approach line—planes have general orientation (electric field). This is the most general case for electric-field interactions. The dynamic effect here is enhanced because the loop offset greatly increases the torques. It is possible that in the latter stages of the approach, each loop will be spinning. If this does occur, then the net force will be a function of time different from that given by the static field variation as a function of separation only.

References

1. Goedecke, G. H., "Classically radiationless motions and possible implications for quantum theory," *Phys. Rev.* **135**: (1B), 13 July 1964, pp B281–288.

2. Mohr, P. J., and B. N. Taylor, "CODATA recommended values of the fundamental physical constants: 1998," *Rev. Mod. Phys.* **72** (2), April 2000, pp 351–495.

3. Menzel, D. H., ed., *Fundamental Formulas of Physics*, Dover Publications, Inc., New York, 1960.

Appendix A. FY01 Director's Research Initiative Proposal

File Number: FY01-CISD

Directorate: Computational and Information Sciences Directorate

Title: Radiationless Moving Charge and Current Distributions Using Clues From Semiclassical Static Electro-Magnitism

Principal Investigator: Dr. Harry J. Auvermann (hauverma@arl.army.mil), U.S. Army Research Laboratory, Computational and Information Sciences Directorate, Battlefield Environment Division, Atmospheric Acoustics and Electro-Optics Propagation Branch, AMSRL-CI-EP, Adelphi Laboratory Center, bldg 202, rm 4G102, ph 301-394-2088, fax 301-394-4797.

Objective: Determine if a magnetic model of the electron has scattering properties matching those measured in electron-electron colliding beam experiments.

Technical Challenge/Background: When the Bohr atom is introduced in a physics curriculum, derivation of the electron motion proceeds under the assumption that this moving charge does not radiate as it traverses the circular or elliptical orbit, even though an accelerating charge is known to radiate energy according to Maxwell's equations. I became aware of an article published in 1964 [1] on radiationless charge-current distributions. The author found that many such distributions exist. A necessary part of producing a radiationless model of the hydrogen atom is a radiationless model of the electron.

I began a study of the properties of the electron starting with the derivation of the classical radius. The semiclassical derivation for this quantity equates the static electric-field energy of a hollow sphere bearing the electron charge to the rest mass energy. For my own benefit, I decided to investigate the static magnetic-field energy of a spinning sphere whose radius is the classical radius, thinking that the magnetic-field energy would be much less than the classical electric-field energy. Using my own approximation for the magnetic-field energy, I was nevertheless very surprised to find that the magnetic-field energy was some 900 times the electric-field energy. Additionally, the peripheral velocity of the sphere had to be many times the speed of light to achieve the required magnetic moment.

Backing off from the classical radius requirement, I sought the radius of a charged loop whose peripheral velocity was the speed of light but still had the correct magnetic moment and field energy. Using my calculation, although approximate, I determined the answer for the model loop radius being what I call the Compton radius, or radius of a circle whose

circumference is the Compton wavelength. I determined also that the required "charged wire" radius (to give an electric-field energy for a Compton radius-sized loop to be equal to the electron rest mass) was a number so small that it defied imagination.

In the intervening years, an article appeared on a colliding-beam experiment (I believe at the European Organization for Nuclear Research) that showed the cross section for electron-electron scattering was at least a factor of 100 less than the classical size. I have not verified or found the reference to this article, but two colleagues have assured me that this result is currently universally accepted in the particle physics community. When the experiment report was published, in light of my "charged wire" radius calculation, I theorized that I may be on the right track with my Compton radius loop model.

Recently, I checked my past calculation. The effort proved surprisingly easy with the benefits of hindsight. The derivation used the commonly available expressions for the various physical constants [2–4]: the fine structure constant, the Bohr radius, the classical radius, the Bohr magneton, the Compton wavelength, the rest mass energy, speed of light in terms of the permeability and permittivity of free space, the magnetic moment of a current loop, the free electron g-factor, the field energy of an inductor, and the inductance of a current loop. The radius was shown to be the Compton radius multiplied by the cube root of a factor consisting of the natural logarithm associated with the inductance times the g-factor squared times the fine structure constant divided by 2π. Because this factor contained the logarithm of the ratio of the current loop radius to the "wire radius" and was to the one-third power, I set it equal to unity and solved for the ratio. The approximate value obtained was the natural base raised to the power 861. As I recall, the ratio I obtained previously for the charge loop was the natural base raised to the power 234. These incredible exponent numbers come about through the reciprocal of the fine structure constant.

Relationship to ARL Mission: The relationship of this effort to the ARL mission is long-term but clearly established. When the U.S. Army fires nuclear weapons, radioactive cleanup is a vital activity on the battlefield. Therefore, the Army needs scientific backup in training and in equipment procurement to responsibly develop operational capability in this area. To a physicist, development of this capability is a natural result of investigations such as is contained in this proposal. The three-element trail is a new understanding of the (1) electron, (2) the atom, and (3) the nucleus. The new understanding arises from incorporating the idea of nonradiating charge or current distributions into fundamental theory. Exploitation of the new idea of the magnetic energy of the electron begins a process whereby the Army, besides attending to its own needs, gives back to the civilian and scientific community something potentially quite significant. To state this long-term mission in a single paragraph is in no way intended to minimize the difficulty expected when performing the work.

Approach: The first requirement is to study the appropriate literature relevant to the high-energy collider experiment result, which will provide the parameters for the theoretical analysis. The next step will be to establish the differences to be expected when a loop is substituted for one of the interacting spherical particles accounting only for electric-field effects. Step by step, the theory will be expanded to the advanced relativistic scattering theory. Indications exist in the literature scanned so far that later experiments took place with polarized particles [5].

It is almost certain that all the steps described here cannot be accomplished in the one year allotted to projects funded under this program. These details are given to establish the overall progression of the intent and mind-set for the work.

Tasks Milestones:

- Oct 00: Complete financial matters. Develop a detailed work plan.
- Jan 01: Complete scenario design. Complete electric-field study.
- Jun 01: Complete magnetic-field study. Begin high-energy study.
- Oct 01: Write final report with recommendations for follow-on work.

Benefits of Successful Completion: Successful completion implies that the theoretical scattering studies are corroborated in some manner by the experimental results. To the extent of this corroboration, a revised model of an electron will be indicated. This revised model can then be used in a more elaborate theoretical scattering investigation than was possible during the limited time period originally allotted to a DRI project. Success in this more elaborate venture will bring the postulation of a radiationless electron model nearer. Success can thus have a ripple effect on models for atoms, leptons other than the electron, baryons, and ultimately the nucleus. I would like to emphasize that these latter effects are complete speculation at present. Ultimate success would be knowledge of the nucleus elaborate enough to suggest methods of radioactivity decay-rate modification [6], which would contribute to more efficient radioactive waste disposal.

Collaborations: Dr. George H. Goedecke, Department of Physics, New Mexico State University, Las Cruces, New Mexico, has agreed to collaborate on this project. Dr. Goedecke is the author of the first article cited in the references to this proposal and has published later findings on the subject. He is a recognized authority on scattering theory, both electromagnetic and quantum mechanical. He is also an author of many papers on other aspects of modern physics. Dr. David A. Ligon of ARL, whose dissertation was in the field of Quantum Electro Dynamics, has agreed to review progress of the work and provide insight within the limits of his other commitments.

Budget:

Salary:	$60,000	Dr. H. J. Auvermann, six man months
Equipment:	$0	
Travel:	$0	
OGA:	$0	
Contract:	$15,000	Dr. G. H. Goedecke, short-term analytical services
Other external:	$0	
Total cost:	$75,000	

Qualifications of Principal Investigator: Auvermann was awarded the Ph.D. degree in Physics/Math in 1957 by the University of Texas at Austin. During most of his career, he has been working in the field of optics. Since 1990, he has been Project Leader for the 6.1 Work Unit Battlefield Acoustic Propagation Research. He initiated the creation of the Turbule Ensemble Model (TEM) of turbulence [7,8], supervised the insertion of TEM into the existing two-dimensional Fast Field Program acoustic propagation model, and supervised the development of the Two-Way Wave Equation Model (TWWEM), a three-dimensional acoustic propagation model.

Literature Search: A search with the use of the elements electron-electron and scattering found some 1500 articles, 90 percent of which deal with semiconductor physics. A search through *Physical Review* failed to locate the article mentioned in the Technical Challenge/Background section. A review article was found [9] as well as several articles on polarization effects other than the one in the reference section [5].

References

1. Goedecke, G. H., "Classically radiationless motions and possible implications for quantum theory," *Phys. Rev.* **135**(1B) (1964), p B281.

2. Abramowitz, M., and I. A. Stegun, *Handbook of Mathematical Functions*, U.S. Government Printing Office, Washington, DC 20402 (1970).

3. Wolfe, William L., and George J. Zissis, *The Infrared Handbook*, U.S. Government Printing Office, Washington, DC 20402 (1978).

4. Menzel, D. H., ed., *Fundamental Formulas of Physics*, Dover Publications, Inc., New York (1960).

5. Shieh, S. Y., "Electron-electron scattering cross section including polarization corrections," *Phys. Lett. B* **B26**(4) (1968).

6. Anderson, J. L., *J. Phy. Chem.* **76** (1972), p 3603.

7. Goedecke, G. H., and H. J. Auvermann, "Acoustic scattering by atmospheric turbules," *J. Acoust. Soc. Am.* **102**(2), Pt. 1 (August 1997).

8. Goedecke, G. H., R. C. Wood, H. J. Auvermann, V. E. Ostashev, D. I. Havelock, and Chueh Ting, "Spectral broadening of sound scattered by advecting atmospheric turbulence," *J. Acoust. Soc. Am.* (May 2001).

9. Panofsky, W.K.H., "Some remarks on the early history of high-energy electron-electron scattering," *Int. J. Mod. Phys. A* **13**(14) (1998), p 2429.

Appendix B. Magnetic Moment of a Spinning Charged Sphere

This appendix will be concerned with deriving an approximation to the magnetic moment of a spinning charged sphere. The method will be to consider the sphere as being made up of a series of loops positioned on the surface of the sphere and add up the contributions to the magnetizing force-field contributions at the center of the sphere. The equivalent current in a loop whose radius is the classical electron radius will be defined as the current that gives the same magnetizing force at its center. The field H_L along the axis of a current loop is given by [1]

$$H_L = \frac{I_L r^2}{2\left[z^2 + r^2\right]^{3/2}} , \tag{B-1}$$

where I_L is the current in the loop and r is the radius of the loop.

The distance from the plane of the loop is the variable z. If the radius of the sphere is r_0 and q_a is the total charge, the surface charge density σ is

$$\sigma = \frac{q_a}{4\pi r_0^2} . \tag{B-2}$$

If the sphere center is at $z = 0$ and the angle ϕ is measured from the positive z-axis, quantities of interest are

$$\begin{aligned} r &= r_0 \sin(\phi); \quad z = r_0 \cos(\phi); \quad I(\phi)d\phi = \frac{\sigma(2\pi r)(r_0 d\phi)(\Omega r)}{(2\pi r)} \\ H_S &= \int_0^\pi d\phi H_L(\phi) = \int_0^\pi d\phi \left(\frac{I(\phi) r^2}{2\left[z^2 + r^2\right]^{3/2}} \right) . \end{aligned} \tag{B-3}$$

The variable H_S is the field at the center of the sphere, and Ω is the angular velocity. The constituents are brought together as

$$\begin{aligned} H_S &= \int_0^\pi d\phi H_L(\phi) = \left(\frac{q_a \Omega r_0}{4\pi r_0^2} \right) \int_0^\pi d\phi \left(\frac{r_0^3 \sin(\phi)^3}{2 r_0^3 \left[\cos(\phi)^2 + \sin(\phi)^2\right]^{3/2}} \right) \\ &= \left(\frac{q_a \Omega}{6\pi r_0} \right) \end{aligned} \tag{B-4}$$

and the integration performed. With equation (B-1) for $z = 0$ and the equivalent loop current I_{cl}, the two are equated and solved for I_{cl} as

$$\begin{aligned} \left(\frac{I_{\mathrm{cl}} r_0^2}{2 r_0^3} \right) &= \left(\frac{q_a \Omega}{6\pi r_0} \right) \\ I_{\mathrm{cl}} &= \left(\frac{q_a \Omega}{3\pi} \right) . \end{aligned} \tag{B-5}$$

[1] Menzel, D. H., ed., *Fundamental Formulas of Physics*, Dover Publications, Inc., New York (1960), p 321.

Equation (B-5) gives the equivalent loop current for a sphere that carries a charge q_a that rotates at an angular velocity of Ω. "Equivalent" means that the magnetic field at the center of the loop is the same as at the center of the sphere. The magnetic moment [2] is shown to be the current times the loop area. Thus the magnetic moment of a spinning charged sphere is

$$\mu^s = 2\pi r_0^2 I_{\rm cl} = \left(\frac{2r_0^2 q_a \Omega}{3}\right) = \left(\frac{2r_0 q_a v^{\rm cl}}{3}\right) , \qquad \text{(B-6)}$$

where $v^{\rm cl}$ is the peripheral velocity of the equivalent current loop to the spherical shell.

[2] Menzel, D. H., ed., *Fundamental Formulas of Physics*, Dover Publications, Inc., New York (1960), p 323.

Appendix C. Potential Interaction Energy of Two Charged Loops

The interaction studied in this appendix is that of two charged coaxial circular loops positioned with their planes parallel. The only force considered is the static electric-field repulsion. The background suggesting the study of the interaction of circular loops has been given in the main text. There the discussion acknowledges the complicated nature of the total interaction of charged and current loops. The restricted interaction equations developed here are intended as a precursor to an extended development to be accomplished at a later date.

Consider the interaction diagram shown in figure C-1. In the figure, the A loop is in the x-y plane and the B loop is in a plane parallel to the x-y plane, with its center a distance $z_b = d$ above the origin O. The various vectors marked by bold symbols are defined as

$$\begin{aligned} \vec{r}_a &= \text{element position vector for A loop} = \hat{x}a\cos(\alpha) + \hat{y}a\sin(\alpha) \\ \vec{r}_b &= \text{element position vector for B loop} = \hat{x}b\cos(\beta) + \hat{y}b\sin(\beta) + \hat{z}d \\ \vec{r}_{ab} &= \vec{r}_b - \vec{r}_a \ , \end{aligned} \tag{C-1}$$

where a is the radius of A loop and b is the radius of B loop. The differential force vector on the charge element at point $\vec{r}_b$ caused by the charge element at point $\vec{r}_a$ is

$$\begin{aligned} d\vec{F}_{ab} &= \left(\frac{1}{4\pi\varepsilon_0 r_{ab}^2}\right)\left(\frac{q_a a\, d\alpha}{2\pi a}\right)\left(\frac{q_b b\, d\beta}{2\pi b}\right)\hat{r}_{ab} = \left(\frac{q_a q_b\, d\alpha\, d\beta}{(2\pi)^2 4\pi\varepsilon_0 r_{ab}^2}\right)\left(\frac{\vec{r}_{ab}}{r_{ab}}\right) \\ r_{ab} &= |\vec{r}_b - \vec{r}_a| = \left[a^2 + b^2 + d^2 - 2ab\cos(\beta - \alpha)\right]^{1/2} \ . \end{aligned} \tag{C-2}$$

The total charges on the loops are q_a and q_b. After integration over the two angles, the total force on B loop will be in the z direction. This is obtained by forming the dot product of equation (C-2) and $\hat{z}$ with the result shown as

$$F_{AB} = \left(\frac{q_a q_b d}{(2\pi)^2 4\pi\varepsilon_0}\right)\int_0^{2\pi} d\alpha \int_0^{2\pi} d\beta r_{ab}^{-3} \ . \tag{C-3}$$

After the α integration is done, the result will be the same for each β so that the β integration will be trivial and β can be set to any value in the α integration. The value is set to zero with the result shown as

Figure C-1. Interaction diagram for two charged loops (A and B). O = origin.

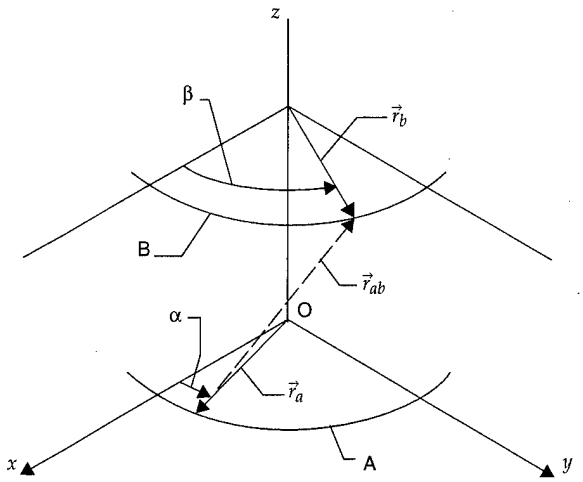

$$
\begin{aligned}
F_{AB} &= \left(\frac{q_a q_b d}{(2\pi)4\pi\varepsilon_0}\right)\int_0^{2\pi} d\alpha\, r_{ab}^{-3}; \quad \text{Let } \bar{b}=\frac{b}{a}; \bar{d}=\frac{d}{a} \\
&= \left(\frac{q_a q_b d}{(2\pi)4\pi\varepsilon_0}\right)\int_0^{2\pi} d\alpha \left[a^2+b^2+d^2-2ab\cos(\alpha)\right]^{-3/2} \qquad \text{(C-4)} \\
&= \left(\frac{2q_a q_b \bar{d}}{(2\pi)4\pi\varepsilon_0 a^2}\right)\int_0^{\pi} d\alpha \left[1+\bar{b}^2+\bar{d}^2-2\bar{b}\cos(\alpha)\right]^{-3/2},
\end{aligned}
$$

along with additional manipulation. The above integral is beginning to look like a standard Elliptic Integral [1], so the variable of integration is changed after use of a trigonometric identity with the result shown as

$$
F_{AB} = \left(\frac{2q_a q_b \bar{d}}{(2\pi)4\pi\varepsilon_0 a^2}\right)\int_0^{\pi/2} d\theta \left[(1-\bar{b})^2+\bar{d}^2+4\bar{b}\sin^2(\theta)\right]^{-3/2}. \qquad \text{(C-5)}
$$

At this point, the identity of the two loops is recognized with the resulting form

$$
F_{AB} = \left(\frac{4q_a^2}{(2\pi)4\pi\varepsilon_0 d^2}\right)\int_0^{\pi/2} d\theta \left[1+D^2\sin^2(\theta)\right]^{-3/2}; \quad D=2\bar{d}^{-1}. \qquad \text{(C-6)}
$$

If this force is integrated from infinity to a particular distance p, then the result will be minus the potential energy $W_{AB}^m(p)$ of B loop in the field of A loop and is shown as

$$
W_{AB}^m(p) = \int_\infty^p dd' F_{AB} = -\left(\frac{4q_a^2}{(2\pi)4\pi\varepsilon_0}\right)\int_\infty^p \left(\frac{dd'}{d'^2}\right)\int_0^{\pi/2} d\theta \left[1+D^2\sin^2(\theta)\right]^{-3/2}. \qquad \text{(C-7)}
$$

It appears that the distance $2a$ has a special role to play, so the variable of the integration will be changed to a unitless quantity with the use of $2a$ as a parameter as

$$
\begin{aligned}
W^m_{AB}(p) &= \left(\frac{-4q_a^2}{(2\pi)4\pi\varepsilon_0}\right)\int_\infty^p\left(\frac{dd'}{d'^2}\right)\int_0^{\pi/2}d\theta\left[1+D^2\sin^2(\theta)\right]^{-3/2};\quad \eta=\frac{d'}{2a}\\
W^m_{AB}(q) &= \left(\frac{-2q_a^2}{(2\pi)4\pi\varepsilon_0 a}\right)\int_\infty^q\left(\frac{d\eta}{\eta^2}\right)\int_0^{\pi/2}d\theta\left[1+\eta^{-2}\sin^2(\theta)\right]^{-3/2};\quad q=\frac{p}{2a} \qquad \text{(C-8)}\\
&= -C_{AB}\int_\infty^q\left(\frac{d\eta}{\eta^2}\right)\int_0^{\pi/2}d\theta\left[1+\eta^{-2}\sin^2(\theta)\right]^{-3/2};\quad C_{AB}=\left(\frac{2q_a^2}{(2\pi)4\pi\varepsilon_0 a}\right).
\end{aligned}
$$

With the anticipation of later investigations, the above integral deserves special attention because the value of the parameter q is to be chosen so that the point of closest approach is to be in the range to match the experimental results. With α now representing the fine-structure constant and the recognition of the loop radius to be the magnetic radius $r_m^{\rm cl}$ or the Compton radius, the classical radius is $\alpha\, r_m^{\rm cl}$. The closest approach should be some 100 times smaller than the classical radius. Therefore, for theoretical purposes, q will be thought of as equal to α^2. It is necessary to break up the integration into two intervals as

$$
\begin{aligned}
\overline{W}^m_{AB}(q) &= \frac{W^m_{AB}(q)}{C_{AB}} = -(L_1+L_2)\\
L_1 &= \int_\infty^1\left(\frac{d\eta}{\eta^2}\right)\int_0^{\pi/2}d\theta\left[1+\eta^{-2}\sin^2(\theta)\right]^{-3/2} \qquad \text{(C-9)}\\
L_2 &= \int_\infty^q\left(\frac{d\eta}{\eta^2}\right)\int_0^{\pi/2}d\theta\left[1+\eta^{-2}\sin^2(\theta)\right]^{-3/2},
\end{aligned}
$$

where the relative potential energy $\overline{W}^m_{AB}(q)$ has been defined also. Solution of the integral L_1 proceeds by an inversion of the order of integration as

$$
\begin{aligned}
L_1 &= \int_\infty^1\left(\frac{d\eta}{\eta^2}\right)\int_0^{\pi/2}d\theta\left[1+\eta^{-2}\sin^2(\theta)\right]^{-3/2} = \int_0^{\pi/2}d\theta\int_\infty^1\left(\frac{d\eta\eta}{\left[\eta^2+\sin^2(\theta)\right]^{3/2}}\right)\\
&= -\int_0^{\pi/2}d\theta\left[1+\sin^2(\theta)\right]^{-1/2} = -K(-1) = -2^{-1/2}K\left(\frac{1}{2}\right), \qquad \text{(C-10)}
\end{aligned}
$$

where $K(m)$ is the Complete Elliptic Integral of the First Kind [1]. Solution of integral L_2 proceeds as

$$
\begin{aligned}
L_2 &= \int_1^q\left(\frac{d\eta}{\eta^2}\right)\int_0^{\pi/2}d\theta\left[1+\eta^{-2}\sin^2(\theta)\right]^{-3/2} = \int_0^{\pi/2}d\theta\int_1^q\left(\frac{d\eta\eta}{\left[\eta^2+\sin^2(\theta)\right]^{3/2}}\right)\\
&= -\int_0^{\pi/2}d\theta\left\{\left[q^2+\sin^2(\theta)\right]^{-1/2}-\left[1+\sin^2(\theta)\right]^{-1/2}\right\} \qquad \text{(C-11)}\\
&= -\left(\frac{1}{(1+q^2)^{1/2}}\right)\int_0^{\pi/2}d\theta\left[\left(\frac{q^2}{(1+q^2)}\right)+\left(\frac{\sin^2(\theta)}{(1+q^2)}\right)\right]^{-1/2}-L_1,
\end{aligned}
$$

[1] Wolfram Research, *Mathematica 3.0 Standard Add-On Packages*, Wolfram Media, Champaign, IL 61820 (1996).

with additional manipulations such as

$$
\begin{aligned}
L_2 &= -\left(\frac{1}{(1+q^2)^{1/2}}\right)\int_0^{\pi/2} d\theta \left[1-\left(\frac{1}{(1+q^2)}\right)\cos^2(\theta)\right]^{-1/2} - L_1 \\
&= -\left(\frac{1}{(1+q^2)^{1/2}}\right)\int_0^{\pi/2} d\theta \left[1-\left(\frac{1}{(1+q^2)}\right)\sin^2(\theta)\right]^{-1/2} - L_1 \qquad \text{(C-12)} \\
&= -\left(\frac{1}{(1+q^2)^{1/2}}\right) K(k) - L_1 \; ; \quad k = (1+q^2)^{-1} \; .
\end{aligned}
$$

Equation (C-13) presents the major result of this derivation

$$
W^m_{AB}(p) = \left(\frac{2k^{1/2}q_a^2 K(k)}{(2\pi)4\pi\varepsilon_0 a}\right) ; \quad k = (1+q^2)^{-1} ; \quad q = \frac{p}{2a} \; , \qquad \text{(C-13)}
$$

which is the expression for the potential energy of two loop model electrons positioned as in figure C-1.

Appendix D. Properties of a Charged Hollow Torus

The derivation in this appendix is shown so as to obtain the equation for the electric field of a charged hollow torus and, from this electric field, find the potential of the torus surface with respect to a zero potential reference at infinity. With the potential and the total charge known, the capacitance is immediately available. The capacitance and the charge then can be used to obtain the field energy of the torus. The approximation is made that the torus is an equipotential surface. Everywhere, the toroidal cross section is a circle. The locus of the centers of the cross-section circles is also a circle.

Figure D-1 shows a three-dimensional diagram of the torus. As indicated in the sectional view of figure D-2, the symbol b represents the radius of the loop and the symbol a represents the radius of the torus cross section.

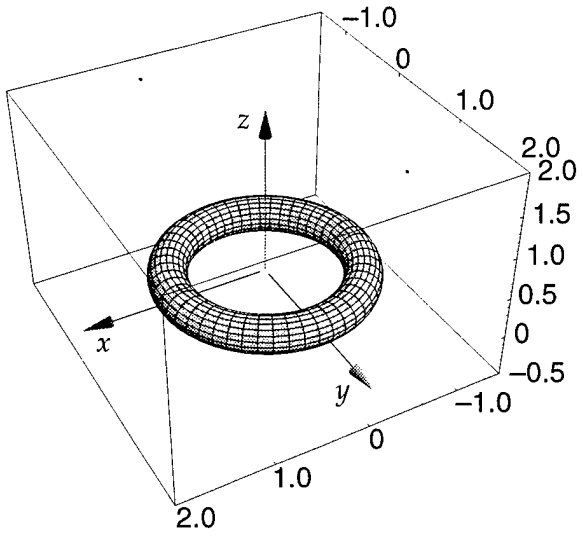

Figure D-1. Three-dimensional diagram of torus.

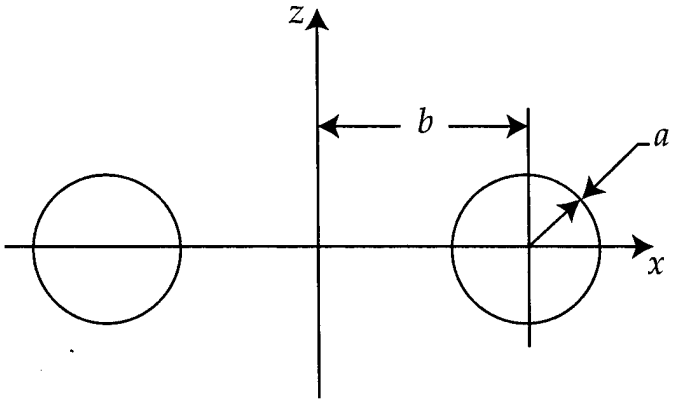

Figure D-2. Sectional diagram of torus through z-axis.

The formula for the surface area of a torus is given in equation (D-1) [1]. In the formula

$$A_t = \pi^2 \left(b'^2 - a'^2\right) \tag{D-1}$$

from the reference, the symbol a' is the inner radius of the torus and the symbol b' is the outer radius of the torus. With the translation of the equation (D-1) formula to the parameters of figure D-2, the equation (D-2) formula is obtained:

$$A_t = (2\pi)^2 ab \; . \tag{D-2}$$

Letting the symbol q_t represent the total charge on the torus, the surface charge density σ_t is

$$\sigma_t = \left(\frac{q_t}{A_t}\right) = \left(\frac{q_t}{(2\pi)^2 ab}\right) \; . \tag{D-3}$$

For the electric field to be found, the electric-flux density D is related to the surface charge density and the direction is assumed normal to the surface. Since the surface is assumed equipotential and since the field is a conservative one, the potential can be obtained by integration of the field along any path from infinity to the surface. The path along the positive x-axis is chosen for its comparative simplicity. By symmetry, this path represents any straight line path in the x-y plane. If the symbol r represents the position along the x-axis, then the integration is from $r = \infty$ to $r = a + b$.

To find the flux density at a point r on the x-axis, assume that a rectangular detector $\bar{D}$ centered on the x-axis (and perpendicular to it) has a dimension w in the y direction and a dimension h in the z direction. The object is to find the dimensions of the patch on the near surface from which issues the flux intercepted by $\bar{D}$. This flux will be augmented by the flux that issues from the patch on the far surface. The far surface is the inner part of the torus, which is on the other side of the z-axis from the near surface. Symbols with the subscript n will apply to the near patch, and symbols with the subscript f will apply to the far patch. Only these two patches need be considered. Justification for this conclusion is discussed later in this appendix. Determination of patch dimensions is facilitated by two diagrams. The first is shown in figure D-3, which depicts the situation in the x-z plane. The rays from the near patch appear to come from the center, marked C_n, of the right-hand trace of the surface in this plane. The detector subtends an angle α_n from this point. The rays from the far patch appear to come from the center, marked C_f, of the left-hand trace of the toroidal surface. The detector subtends an angle α_f from this point.

Equation (D-4) shows the calculation of these two-patch dimensions:

$$\begin{aligned} \alpha_n &= \left(\frac{h}{r-b}\right); \qquad h_n = \left(\frac{ha}{r-b}\right) \\ \alpha_f &= \left(\frac{h}{r+b}\right); \qquad h_f = \left(\frac{ha}{r+b}\right) \; . \end{aligned} \tag{D-4}$$

[1] Spiegel, M. R., *Mathematical Handbook of Formulas and Tables*, Schaum's Outline Series, McGraw-Hill, Inc., New York (1968), 34th Printing (1995), p 10.

Figure D-3. Patch dimensions in x-z plane.

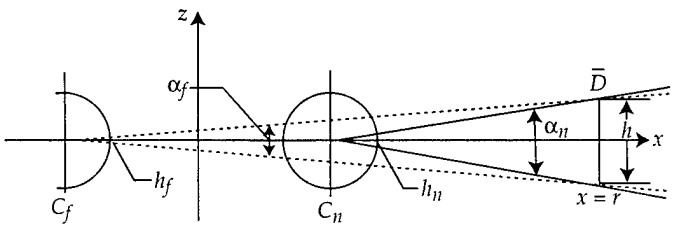

The second patch dimension diagram is shown in figure D-4, which depicts the situation in the x-y plane. The rays from both patches appear to come from the loop center, which is the coordinate system origin. This is seen easily for the near patch. It is also true for the far patch, because the normal rays tend to focus the flux at the origin in this plane. The detector subtends an angle β_n from this point for the near patch. The detector subtends an angle β_f for the far patch. Although for $\beta_n = \beta_f$, the patch dimensions are different.

The calculation of these two-patch dimensions is

$$\beta_n = \left(\frac{w}{r}\right); \quad w_n = \left(\frac{w(b+a)}{r}\right); \quad w_f = \left(\frac{w(b-a)}{r}\right). \tag{D-5}$$

The flux from the entire charge in a patch proceeds outward, as justified at the end of this appendix. The partial flux at the detector from the two patches designated by $\Delta F_{\bar{D}}$ is

$$\begin{aligned} \Delta F_{\bar{D}} &= \sigma_t(h_n w_n + h_f w_f) = \\ &= \left(\frac{q_t}{(2\pi)^2 ab}\right)\left(\left(\frac{hb}{r-a}\right)\left(\frac{w(a+b)}{r}\right) + \left(\frac{hb}{r+a}\right)\left(\frac{w(a-b)}{r}\right)\right). \end{aligned} \tag{D-6}$$

The electric-flux density is then obtained by dividing the flux by the detector area as

$$D(r) = \left(\frac{q_t}{(2\pi)^2 ar}\right)\left(\left(\frac{a+b}{r-a}\right) + \left(\frac{a-b}{r+a}\right)\right). \tag{D-7}$$

Dividing by the electric constant ε_0 gives the electric field as

$$E(r) = \left(\frac{2q_t}{(2\pi)^2 \varepsilon_0 r}\right)\left(\frac{r+b}{r^2-a^2}\right) = \left(\frac{2[1+(b/r)]}{\pi}\right)\left(\frac{q_t}{4\pi\varepsilon_0(r^2-a^2)}\right). \tag{D-8}$$

At great distances where r is much greater than a or b, the electric field is seen to be the same as that from a point charge except for the $2/\pi$ factor in the first bracket. To obtain the potential ϕ_t, assume that the charge is positive and accumulate the energy necessary to move a unit positive charge from infinity to $r = a + b$ through the field of equation (D-8) as

$$\phi_t = \left(\frac{2}{\pi}\right)\left(\frac{q_t}{4\pi\varepsilon_0}\right)\int_{\infty}^{a+b} dr \left(\frac{r+b}{r(r^2-a^2)}\right). \tag{D-9}$$

Figure D-4. Patch dimensions in x-y plane.

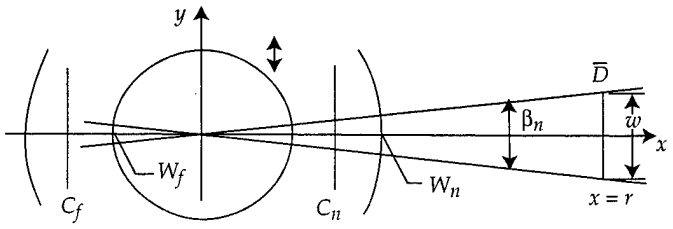

To solve the integral, substitute for the variable of integration $a\tan(\theta)$ as

$$\begin{aligned}\phi_t &= Q_t \int_{\pi/2}^{\theta_t} d\theta \left(\frac{\sec(\theta)^2[\tan(\theta)+b/a]}{\tan(\theta)[\tan(\theta)^2-1]} \right); \quad \theta_t = \arctan(1+b/a) \\ &= \left(\frac{Q_t}{a}\right) \int_{\pi/2}^{\theta_t} d\theta \left(\frac{[a\sin(\theta)+b\cos(\theta)]}{\sin(\theta)\cos(2\theta)} \right); \quad Q_t = \left(\frac{2}{\pi}\right)\left(\frac{q_t}{4\pi\varepsilon_0 a}\right) . \end{aligned} \tag{D-10}$$

Further manipulations are carried out by

$$\begin{aligned}\phi_t &= \left(\frac{Q_t\,(a^2+b^2)^{1/2}}{a} \right) \int_{\pi/2}^{\frac{\pi}{4}+\delta} d\theta \left(\frac{\sin(\theta+\gamma)}{\sin(\theta)\cos(2\theta)} \right); \quad \theta_t = \frac{\pi}{4}+\delta \\ \tan(\gamma) &= \frac{b}{a}\,; \quad \tan\left(\frac{\pi}{4}+\delta\right) = 1+b/a\,; \quad \tan(\delta) = \left(\frac{b/a}{2+b/a}\right) . \end{aligned} \tag{D-11}$$

The integration result is shown as [2]

$$\begin{aligned} I &= \int_{\pi/2}^{\frac{\pi}{4}+\delta} d\theta \left(\frac{\sin(\theta+\gamma)}{\sin(\theta)\cos(2\theta)} \right) \\ &= \left(\frac{1}{2}\right) \left\{ \cos(\gamma) \ln\left[\frac{\cos(\delta)}{\sin(\delta)}\right] + \sin(\gamma) \ln\left[\frac{(\cos(\delta)+\sin(\delta))^2}{4\cos(\delta)\sin(\delta)}\right] \right\} \\ &= \left(\frac{1}{2(a^2+b^2)^{1/2}}\right) \left\{ a\ln\left[\frac{a}{b}\right] + b\ln\left[\frac{(2a+b)(a+b)}{2ab}\right] \right\} . \end{aligned} \tag{D-12}$$

Substituting in equation (D-11), the final expression for the potential is

$$\begin{aligned}\phi_t &= \left(\frac{1}{\pi}\right)\left(\frac{q_t}{4\pi\varepsilon_0 a}\right) \left\{ \ln\left[\frac{a}{b}\right] + \left(\frac{b}{a}\right) \ln\left[\frac{(2a+b)(a+b)}{2ab}\right] \right\} \\ &= \left(\frac{1}{\pi}\right)\left(\frac{q_t}{4\pi\varepsilon_0 a}\right) \left\{ \left(1+\frac{b}{a}\right) \ln\left[\frac{a}{b}\right] + \left(\frac{b}{a}\right) \ln\left[\left(1+\frac{b}{2a}\right)\left(1+\frac{b}{a}\right)\right] \right\} . \end{aligned} \tag{D-13}$$

For large a/b (and small b/a), the $\ln(a/b)$ term is dominent so that an approximate potential is given by

$$\tilde{\phi}_t = \left(\frac{1}{\pi}\right)\left(\frac{q_t}{4\pi\varepsilon_0 a}\right) \ln\left[\frac{a}{b}\right] . \tag{D-14}$$

[2] Wolfram, S., *MATHEMATICA*, 2nd ed., Addison-Wesley, New York (1991).

The equation for the capacitance C is [3]

$$C = \frac{q}{\Delta\phi}; \qquad C_t = \frac{q_t}{\phi_t} \tag{D-15}$$

in terms of the charge q and the potential difference $\Delta\phi$. The capacitance C_t of the torus is also shown in equation (D-15). The energy W stored in a capacitance [3] is given in two forms as

$$W = \frac{C(\Delta\phi)^2}{2} = \frac{q^2}{2C} \, . \tag{D-16}$$

With the use of the second form and substituting quantities defined in equation (D-13), the formula for the electric-field energy of the torus W_t is shown as

$$\begin{aligned} W_t &= \frac{q_t^2}{2C_t} \\ &= \left(\frac{1}{2\pi}\right)\left(\frac{q_t^2}{4\pi\varepsilon_0 a}\right)\left\{\left(1+\frac{b}{a}\right)\ln\left[\frac{a}{b}\right] + \left(\frac{b}{a}\right)\ln\left[\left(1+\frac{b}{2a}\right)\left(1+\frac{b}{a}\right)\right]\right\} . \end{aligned} \tag{D-17}$$

It is instructive to use the approximate formula for the torus potential, equation (D-14), to obtain an idea of the magnitude of this electric-field energy for the torus configuration calculated in the main text of this report. The approximate value for the electric-field energy of the torus $\tilde{W}_t$ is

$$\tilde{W}_t = \left(\frac{1}{2\pi}\right)\left(\frac{q_t^2}{4\pi\varepsilon_0 a}\right)\ln\left[\frac{a}{b}\right] \, . \tag{D-18}$$

From equation (23) in the main text, the loop radius is given as the Compton radius, and from equation (26), the approximate value of the loop parameter ρ_m is given. These values are shown as

$$\frac{r_C}{\tilde{r}_t} = \tilde{\rho}_m = \exp\left(\frac{2\pi}{\alpha}\right) \, . \tag{D-19}$$

The variable r_C is identified with the variable b in equation (D-18), and the variable $\tilde{r}_t$ is identified with the variable a in equation (D-18). With the appropriate substitutions made in equation (D-18), the result is shown as

$$\tilde{W}_t = \left(\frac{1}{2\pi}\right)\left(\frac{q_t^2}{4\pi\varepsilon_0 r_C}\right)\ln\left[\frac{r_C}{\tilde{r}_t}\right] = \left(\frac{1}{2\pi}\right)\left(\frac{q_t^2}{4\pi\varepsilon_0 r_C}\right)\left(\frac{2\pi}{\alpha}\right) \, . \tag{D-20}$$

Consolidating equation (D-20) and noting the relation between the Compton radius and the classical radius r_0 from equation (7) in the main text, one can show the result as

$$\tilde{W}_t = \left(\frac{q_t^2}{4\pi\varepsilon_0 r_0}\right) = w_e \, . \tag{D-21}$$

[3] Menzel, D. H., ed., *Fundamental Formulas of Physics*, Dover Publications, Inc., New York (1960), p 318.

The final identification is made with w_e of equation (8) in the main text, which is the rest mass energy of the electron. Thus we find that the approximate electric-field energy of the present configuration of the hollow torus is the same as that of the classical electron model. This information has only been mentioned in the main text of this report because an appropriate allocation of the rest mass energy between the electric and magnetic fields has not been determined.

That only two patches are needed for finding the electric field of a torus may be concluded by considering the situation wherein charge radiates electric flux both outward (as with the derivation just shown) and inward. The reduction in flux by a factor of two is made up by the inclusion of four patches instead of two. In reference to figure D-3, the focusing effect in the z-direction causes the flux from the left-hand patches of the tubes to be redistributed onto the right-hand patches, thus effectively augmenting the outward-moving flux. In figure D-4, this same effect occurs in the y-direction. The inward-moving flux from the left-hand portion of the torus moves through the focus point (the coordinate origin) and redistributes itself on the right-hand portion of the torus. A further point can be made concerning the net flux within the torus: With flux being focused in both directions inside the torus, the net flux at each point balances to zero in figure D-3, indicating zero field, considering only one circle. The effect of the flux from one circle on the other circle has not been included. Thus, the assumption that the surface is equipotential only becomes true as the ratio a/b approaches zero. In figure D-4, in the x-y plane, the focused flux from both sides balances to zero everywhere inside the loop, again indicating zero field in this plane.

Distribution

Admnstr
Defns Techl Info Ctr
ATTN DTIC-OCP
8725 John J Kingman Rd Ste 0944
FT Belvoir VA 22060-6218

DARPA
ATTN S Welby
3701 N Fairfax Dr
Arlington VA 22203-1714

Mil Asst for Env Sci Ofc of the Undersec of
Defns for Rsrch & Engrg R&AT E LS
Pentagon Rm 3D129
Washington DC 20301-3080

Ofc of the Secy of Defns
ATTN ODDRE (R&AT)
The Pentagon
Washington DC 20301-3080

Ofc of the Secy of Defns
ATTN OUSD(A&T)/ODDR&E(R) R J Trew
3080 Defense Pentagon
Washington DC 20301-7100

AMCOM MRDEC
ATTN AMSMI-RD W C McCorkle
Redstone Arsenal AL 35898-5240

US Army TRADOC
Battle Lab Integration & Techl Dirctrt
ATTN ATCD-B
FT Monroe VA 23651-5850

US Military Acdmy
Dept of Mathematical Sci
ATTN MAJ L G Eggen
West Point NY 10996-1786

US Military Acdmy
Mathematical Sci Ctr of Excellence
ATTN MADN-MATH MAJ M Huber
Thayer Hall
West Point NY 10996-1786

Natl Ground Intllgnc Ctr
Army Foreign Sci Tech Ctr
ATTN CM
220 7th Stret NE
Charlottesville VA 22901-5396

Natl Security Agcy
ATTN W21 Longbothum
9800 Savage Rd
FT George G Meade MD 20755-6000

Dir for MANPRINT
Ofc of the Deputy Chief of Staff for Prsnnl
ATTN J Hiller
The Pentagon Rm 2C733
Washington DC 20301-0300

Sci & Technlgy
101 Research Dr
Hampton VA 23666-1340

SMC/CZA
2435 Vela Way Ste 1613
El Segundo CA 90245-5500

TECOM
ATTN AMSTE-CL
Aberdeen Proving Ground MD 21005-5057

US Army ARDEC
ATTN AMSTA-AR-TD
Bldg 1
Picatinny Arsenal NJ 07806-5000

US Army Corps of Engrs
Engr Topographics Lab
ATTN CETEC-TR-G P F Krause
7701 Telegraph Rd
Alexandria VA 22315-3864

US Army CRREL
ATTN CRREL-GP R Detsch
72 Lyme Rd
Hanover NH 03755-1290

Distribution (cont'd)

US Army Dugway Proving Ground
ATTN STEDP 3
Dugway UT 84022-5000

US Army Field Artillery Schl
ATTN ATSF-TSM-TA
FT Sill OK 73503-5000

US Army Infantry
ATTN ATSH-CD-CS-OR E Dutoit
FT Benning GA 30905-5090

US Army Info Sys Engrg Cmnd
ATTN AMSEL-IE-TD F Jenia
FT Huachuca AZ 85613-5300

US Army Natick RDEC
Acting Techl Dir
ATTN SBCN-T P Brandler
Natick MA 01760-5002

US Army OEC
ATTN CSTE-AEC-FSE
4501 Ford Ave Park Center IV
Alexandria VA 22302-1458

US Army Simulation Train & Instrmntn Cmnd
ATTN AMSTI-CG M Macedonia
ATTN J Stahl
12350 Research Parkway
Orlando FL 32826-3726

US Army Soldier & Biol Chem Cmnd
Dir of Rsrch & Techlgy Dirctrt
ATTN SMCCR-RS I G Resnick
Aberdeen Proving Ground MD 21010-5423

US Army Tank-Automtv Cmnd RDEC
ATTN AMSTA-TR J Chapin
Warren MI 48397-5000

US Army TRADOC
Anal Cmnd—WSMR
ATTN ATRC-WSS-R
White Sands Missile Range NM 88002

US Army TRADOC
ATTN ATCD-FA
FT Monroe VA 23651-5170

Nav Air War Cen Wpn Div
ATTN CMD 420000D C0245 A Shlanta
1 Admin Cir
China Lake CA 93555-6001

Nav Surfc Warfare Ctr
ATTN Code B07 J Pennella
17320 Dahlgren Rd Bldg 1470 Rm 1101
Dahlgren VA 22448-5100

Nav Surfc Weapons Ctr
ATTN Code G63
Dahlgren VA 22448-5000

USAF Rsrch Lab Phillips Lab
Atmos Sci Div Geophysics Dirctrt
Hanscom AFB MA 01731-5000

US Air Force
ATTN Weather Techl Lib
151 Patton Ave Rm 120
Asheville NC 28801-5002

USAF Rome Lab Tech
ATTN Corridor W Ste 262 RL SUL
26 Electr Pkwy Bldg 106
Griffiss AFB NY 13441-4514

NASA Marshal Spc Flt Ctr
Atmos Sci Div
ATTN Code ED 41 1
Huntsville AL 35812

Hicks & Assoc Inc
ATTN G Singley III
1710 Goodrich Dr Ste 1300
McLean VA 22102

Natl Ctr for Atmos Rsrch
ATTN NCAR Library Serials
PO Box 3000
Boulder CO 80307-3000

Distribution (cont'd)

NCSU
ATTN J Davis
PO Box 8208
Raleigh NC 27650-8208

Pacific Mis Test Ctr Geophysics Div
ATTN Code 3250
Point Mugu CA 93042-5000

US Army Rsrch Lab
ATTN AMSRL-IS-EW
White Sands Missile Range NM 88002-5501

Director
US Army Rsrch Lab
ATTN AMSRL-RO-D JCI Chang
ATTN AMSRL-RO-EN W D Bach
PO Box 12211
Research Triangle Park NC 27709

US Army Rsrch Lab
ATTN AMSRL-D D R Smith
ATTN AMSRL-DD J M Miller
ATTN AMSRL-CI-AI-R Mail & Records Mgmt
ATTN AMSRL-CI-AP Techl Pub (2 copies)
ATTN AMSRL-CI-LL Techl Lib (2 copies)
ATTN AMSRL-CI-EP H J Auvermann (15 copies)
Adelphi MD 20783-1197

REPORT DOCUMENTATION PAGE

Form Approved
OMB No. 0704-0188

1. AGENCY USE ONLY *(Leave blank)*	2. REPORT DATE	3. REPORT TYPE AND DATES COVERED
	February 2001	Final, June to August 2000

4. TITLE AND SUBTITLE An Elementary Electron Model for Electron-Electron Scattering Based On Static Magnetic Field Energy

5. FUNDING NUMBERS
DA PR: B53A
PE: 61102A

6. AUTHOR(S) Harry J. Auvermann

7. PERFORMING ORGANIZATION NAME(S) AND ADDRESS(ES)
U.S. Army Research Laboratory
Attn: AMSRL-CI-EP email: hauverma@arl.army.mil
2800 Powder Mill Road
Adelphi, MD 20783-1197

8. PERFORMING ORGANIZATION REPORT NUMBER
ARL-TR-2332

9. SPONSORING/MONITORING AGENCY NAME(S) AND ADDRESS(ES)
U.S. Army Research Laboratory
2800 Powder Mill Road
Adelphi, MD 20783-1197

10. SPONSORING/MONITORING AGENCY REPORT NUMBER

11. SUPPLEMENTARY NOTES
ARL PR: OFEJ60
AMS code: 61110253A11

12a. DISTRIBUTION/AVAILABILITY STATEMENT Approved for public release; distribution unlimited.

12b. DISTRIBUTION CODE

13. ABSTRACT *(Maximum 200 words)*

Electron motion paths that exhibit zero radiation in a Maxwell's equation solution have been reported. Such paths, require a radiationless model of the electron itself, such as the charged hollow sphere. When the electric-field energy of this model is set equal to the rest mass energy of the electron, the radius of the resulting sphere is called the "classical electron radius." Analysis reveals that the static magnetic-field energy of the classical model is many times the electron rest mass energy when the sphere is given an angular velocity large enough to exhibit the electron magnetic moment. The necessary angular velocity produces a peripheral velocity many times the speed of light. A classical model with a peripheral velocity near the speed of light is a loop whose radius is the Compton wavelength divided by 2π; such a loop has a very small dimension perpendicular to the loop plane. Experiments reveal point-like electron scattering properties down to at least 1/100 of the classical radius. The small transverse dimensions of the loop model indicate similar scattering results. Recently, a proposal was submitted to investigate the scattering properties of interacting loops. Because of limited proposal length, derivation of loop model equations could not be included. This report contains the details of the analysis.

14. SUBJECT TERMS	15. NUMBER OF PAGES
Current loop, classical scattering, rest mass energy	42
	16. PRICE CODE

17. SECURITY CLASSIFICATION OF REPORT	18. SECURITY CLASSIFICATION OF THIS PAGE	19. SECURITY CLASSIFICATION OF ABSTRACT	20. LIMITATION OF ABSTRACT
Unclassified	Unclassified	Unclassified	UL